


COMPUTED TOMOGRAPHY



# Diagnostic performance of photon-counting detector CT for differentiation between adrenal adenomas and metastases

Stefanie Bette<sup>1</sup>, Franka Risch<sup>1</sup>, Luca Canalini<sup>1</sup>, Judith Becker<sup>1</sup>, Eva V. Leithner<sup>1</sup>, Adrian Huber<sup>1</sup>, Mark Haerting<sup>1</sup>, Bertram Jehs<sup>1</sup>, Claudia Wollny<sup>1</sup>, Florian Schwarz<sup>2</sup>, Kartikay Tehlan<sup>1</sup>, Christian Scheurig-Muenkler<sup>1</sup>, Thomas Wendler<sup>1,3,4</sup>, Thomas Kroencke<sup>1,5\*</sup>  and Josua A. Decker<sup>1</sup>

## Abstract

**Objectives** Aim of this study was to assess the value of virtual non-contrast (VNC) reconstructions in differentiating between adrenal adenomas and metastases on a photon-counting detector CT (PCD-CT).

**Material and methods** Patients with adrenal masses and contrast-enhanced CT scans in portal venous phase were included. Image reconstructions were performed, including conventional VNC (VNC<sub>Conv</sub>) and PureCalcium VNC (VNC<sub>PC</sub>), as well as virtual monochromatic images (VMI, 40–90 keV) and iodine maps. We analyzed images using semi-automatic segmentation of adrenal lesions and extracted quantitative data. Logistic regression models, non-parametric tests, Bland–Altman plots, and a random forest classifier were used for statistical analyses.

**Results** The final study cohort consisted of 90 patients (36 female, mean age 67.8 years [range 39–87]) with adrenal lesions (45 adenomas, 45 metastases). Compared to metastases, adrenal adenomas showed significantly lower CT-values in VNC<sub>Conv</sub> and VNC<sub>PC</sub> ( $p=0.007$ ). Mean difference between VNC and true non-contrast (TNC) was 17.67 for VNC<sub>Conv</sub> and 14.85 for VNC<sub>PC</sub>. Random forest classifier and logistic regression models both identified VNC<sub>Conv</sub> and VNC<sub>PC</sub> as the best discriminators. When using 26 HU as the threshold in VNC<sub>Conv</sub> reconstructions, adenomas could be discriminated from metastases with a sensitivity of 86.7% and a specificity of 75.6%.

**Conclusion** VNC algorithms overestimate CT values compared to TNC in the assessment of adrenal lesions. However, they allow a reliable discrimination between adrenal adenomas and metastases and could be used in clinical routine in near future with an increased threshold (e.g., 26 HU). Further (multi-center) studies with larger patient cohorts and standardized protocols are required.

**Clinical relevance statement** VNC reconstructions overestimate CT values compared to TNC. Using a different threshold (e.g., 26 HU compared to the established 10 HU), VNC has a high diagnostic accuracy for the discrimination between adrenal adenomas and metastases.

## Key Points

- Virtual non-contrast reconstructions may be promising tools to differentiate adrenal lesions and might save further diagnostic tests.

\*Correspondence:  
Thomas Kroencke  
thomas.kroencke@uk-augsburg.de  
Full list of author information is available at the end of the article

- *The conventional and a new calcium-preserving virtual non-contrast algorithm tend to systematically overestimate CT-values compared to true non-contrast images.*
- *Therefore, increasing the established threshold for true non-contrast images (e.g., 10HU) may help to differentiate between adrenal adenomas and metastases on contrast-enhanced CT.*

**Keywords** Photon-counting detector computed tomography, Adrenal adenomas, Virtual non-contrast

## Introduction

The incidental detection of adrenal lesions has increased over the past decades due to improved imaging techniques and increasing numbers of CT scans, with an estimated prevalence of 4–8% on abdominal CT scans [1–4]. Recent guidelines from the American College of Radiology provide an algorithm for the workup of incidentally detected adrenal lesions  $\geq 1$  cm [4]. Depending on size, the presence of indeterminate or high-risk imaging features, and history of cancer, either a follow-up or an adrenal CT is recommended [4]. An adrenal CT consists of a pre-contrast scan, a portal venous phase, and a late phase (15 min) [4, 5].

Adrenal adenomas can be differentiated from metastases by low CT values on unenhanced CT ( $< 10$  HU) or by rapid washout between portal venous and late contrast phases (relative washout  $> 60\%$ ) [1, 4, 6]. In clinical routine, adrenal lesions are often detected on contrast-enhanced CT scans and therefore cannot be confidently identified as adenomas. In these cases, further imaging (e.g., an adrenal CT) or follow-up is recommended [4], resulting in additional radiation dose to the patient or a delayed clarification with the potential psychological burden respectively.

Previous studies on dual-energy CT (DECT) have addressed the value of virtual non-contrast (VNC) images for the assessment of adrenal lesions [1, 7–9]. However, most studies indicated that VNC overestimated CT values compared to true non-contrast (TNC). VNC series were therefore not recommended for routine clinical use.

In 2021, the photon-counting detector (PCD) technology was introduced. It enables the direct conversion of single X-ray photons into an electric signal, resulting in the reduction of electronic noise and the availability of broad spectral imaging with each scan [10]. A recent study assessed the value of VNC reconstructions on a PCD-CT for the evaluation of adrenal adenomas. However, similar to previous studies, VNC showed an over- or underestimation of CT values compared to TNC [11].

Besides the conventional VNC ( $VNC_{Conv}$ ), a new algorithm is available for creating VNC series: the Pure-Calcium algorithm ( $VNC_{PC}$ ). Because iodine has a similar attenuation as calcium, calcium contrast is partially removed in  $VNC_{Conv}$  series. To address this problem and preserve calcium contrast,  $VNC_{PC}$  creates a

calcium mask before material differentiation. Recent studies analyzing this algorithm reported more consistent VNC values not only for calcified lesions but also for soft tissue [12–14].

Aims of this study were (i) to analyze the conventional VNC ( $VNC_{Conv}$ ) and the new VNC algorithm ( $VNC_{PC}$ ) for assessment of adrenal lesions in comparison to TNC and (ii) to analyze the value of spectral imaging for the discrimination of adrenal lesions on contrast-enhanced CT scans.

## Material and methods

### Study population

We searched the local database consisting of patients with suspected malignancy and a contrast-enhanced CT of the abdomen between 04/2021 and 09/2022.

The local Medical Research and Ethics Committee (MREC) approved this retrospective single-center study and waived the need for informed consent for the patients included in the retrospective cohort (protocol number: 23–0451).

Inclusion criteria for the retrospective cohort were as follows: (1) age  $\geq 18$  years, (2) contrast-enhanced CT of the abdomen on a dual-source photon-counting detector CT (PCD-CT) between 04/2021 and 09/2022 in portal venous phase, (3) presence of an adrenal lesion  $\geq 1$  cm.

### Reference standard

The definition of lesions as adenomas or metastases was performed as described previously [1, 4]. Lesions were diagnosed as adenomas when (1) unenhanced CT showed CT values  $\leq 10$  HU or (2) size did not change during at least 6 months or (3) abdominal MRI including chemical shift imaging showed signal drop in opposed-phase or (4) the lesion showed an absolute washout  $> 60\%$  in multiphasic CT. Lesions were diagnosed as metastases when (1) size of the lesion changed within 6 months or (2) abnormal [ $^{18}F$ ]FDG uptake was shown at PET/CT in a known malignancy.

### Imaging protocol

All PCD-CT scans were performed on a dual-source photon-counting detector CT (NAEOTOM Alpha, Siemens Healthineers) as routine clinical acquisitions using a monophasic contrast injection protocol in portal

venous phase. Each patient received a contrast bolus of 100 mL (Ultravist 300 mgI/mL, Bayer) that was injected via an antecubital vein (flow rate 4.0 mL/s) and followed by a saline bolus of 30 mL. Images were acquired in portal venous contrast phase (after fixed delay of 75 s after contrast injection).

All patients were scanned craniocaudally in a supine position during a single breath-hold. The following parameters were applied: acquisition mode with readout of spectral information (Abdomen QuantumPlus, Siemens Healthineers), 120-kV tube voltage, 0.5 s or 0.25 s, rotation time,  $144 \times 0.4$  mm collimation.

A part of the patient cohort also received true non contrast CT, either within the same protocol prior to contrast application or within a separate acquisition, e.g., during FDG-PET or radiation planning.

### Image reconstruction

CTs were reconstructed from image raw data using a dedicated research software (ReconCT 16.0, Siemens Healthineers). For each patient, two VNC series, one conventional ( $VNC_{conv}$ ) and one pureCalcium ( $VNC_{PC}$ ) at a virtual monoenergetic level of 70 keV, iodine maps, and virtual monoenergetic image (VMI) series from 40 to 90 keV in 10-keV increments were reconstructed. The slice thickness and increment were 1.0 and 0.5 mm. A soft tissue kernel optimized for quantitative evaluation, Qr40, was used with an iteration strength of 3. Image

reconstruction of TNC images was performed using SyngoVia (Syngo.via VB60A, Siemens Healthineers) and same slice thickness and increment as in the PCD-CT.

### Image analysis

Semiautomatic segmentation of adrenal lesions was performed by a board-certified radiologist (S.B.) with 7 years of experience in abdominal CT imaging using open-source software 3D Slicer (<http://www.slicer.org> [15]) (Fig. 1). Quantitative data were extracted after lesion segmentation for all reconstructions (VMI 40–90 keV,  $VNC_{conv}$ ,  $VNC_{PC}$ , and iodine maps) using pyradiomics (version 3.1.0 [16]). First-order features (mean HU values) were used for further analyses. True non-contrast (TNC) images were available for 49/90 patients (for 14/45 metastasis and 35/45 adenomas).

### Statistical analysis

Analysis of descriptive data and statistical analyses were performed using R (R Statistics, version 4.3.1, R Core Team, [17]), RStudio (version 2023.06.2 [18]), and Python 3.7.1 ([www.python.org](http://www.python.org)). Shapiro–Wilk tests were performed to check for normal distribution. Non-normally distributed data are presented as median and interquartile range (IQR), normally distributed data as mean ( $\pm$  standard deviation). Mann–Whitney *U* tests (non-normally distributed data) or *t*-tests (normally distributed data) were performed to compare between two

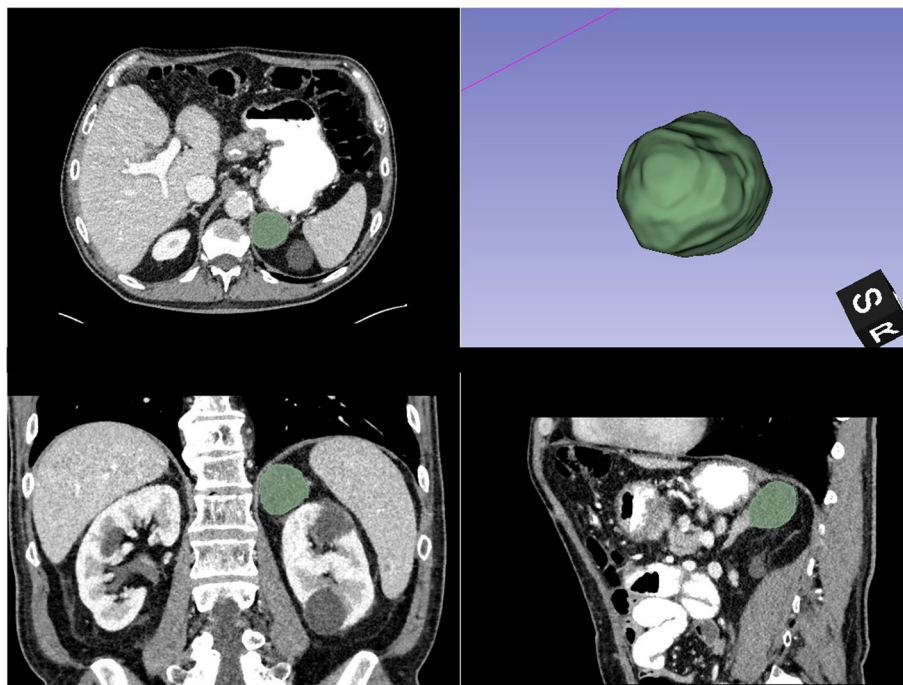


**Fig. 1** Example of semiautomatic segmentation of a left adrenal adenoma using 3D Slicer

groups. Bonferroni correction was performed for multiple testing. Bland–Altman plots were used to describe the similarity between VNC and TNC. Logistic regression models with imaging features (HU values from spectral data) as independent variables and outcome (adenoma vs. metastasis) as dependent variable were performed after splitting the cohort into training and test cohort (80/20). Five models were randomly built on the training cohort (fivefold cross-validation). After 5 models were trained and validated, the method gave as final trained model the one that obtained the best results. This model was then applied on the test cohort. ROC analyses were performed in R using the *pROC-package*. Data are shown for all established models (folds 1–5) as well as for the selected best model (test set). Area under the curve (AUC) is shown for the model that was applied on the test cohort. The optimal cutoff value was determined using the *cutpointr-package* in R. For feature selection, the Boruta package was applied in R. The Boruta algorithm is a wrapper method for feature selection and often applied in radiomics analyses [19]. The algorithm uses a random forest (RF)–based classification model to select the most important features. Statistically significant differences were assumed at  $p$ -values  $\leq 0.05$ .

## Results

### Patient population

From the local database, 110 patients with adrenal lesions were identified. We excluded patients due to missing ground truth ( $n=10$ ), lesions too small to measure ( $n=4$ ), missing contrast-enhanced scan ( $n=1$ ), diagnosis of adrenal carcinoma ( $n=1$ ), and missing raw data ( $n=4$ ).

Finally, 90 patients (36 female assigned at birth, mean age 67.8 years [range 39–87]) were included in this study. Twenty-six patients had bilateral adrenal lesions; in these cases, we analyzed the left side (except for one case with calcification in the left adrenals). Baseline characteristics are shown in Table 1.

### Quantitative analysis

Adrenal adenomas showed significantly lower median CT values in VNC<sub>Conv</sub> reconstructions (18.15 [12.92–24.26] vs. 31.28 [26.00–35.89],  $p=0.007$ ) and in VNC<sub>PC</sub> reconstructions (16.00 [11.02–21.56] vs. 27.22 [22.59–30.64],  $p=0.007$ ) compared to adrenal metastases (Fig. 2, Table 2).

For patients with available TNC images ( $n=49$ ; metastasis = 14, adenoma = 35), Bland Altman plots showed a mean difference of 14.85 for VNC<sub>PC</sub> reconstructions and of 17.67 for VNC<sub>Conv</sub> reconstructions with higher values for both VNC algorithms compared to TNC (Fig. 3).

### Feature selection

Using the Boruta random forest method for feature selection, VNC<sub>Conv</sub> and VNC<sub>PC</sub> were selected as the features with the highest importance (Table 3, Fig. 4). Also, iodine maps as well as VMI 80 and 90 keV were important features in this model yet with lower importance.

### Logistic regression models

Logistic regression models showed that use of all available spectral data had the best ability to discriminate between adrenal adenomas and adrenal metastases (AUC = 0.938) (Fig. 5). Used independently, TNC

**Table 1** Baseline characteristics

	Metastasis ( $n=45$ )	Adenoma ( $n=45$ )	$p$ value
$n$ , female (%)	20 (44.4)	16 (35.6)	0.395
Age, years (mean [range])	67.8 (39–87)	67.8 (45–87)	1.000
Side (measured), left (%)	35 (77.8)	37 (82.2)	0.603
BMI, kg/m <sup>2</sup> (median [IQR])	24.18 (21.19–29.67)	27.49 (24.87–30.51)	0.051
CTDI <sub>Vol</sub> , mGy·cm, median [IQR]	7.37 (6.06–10.06)	8.67 (6.27–10.90)	0.418
Cancer origin	Lung cancer: $n=28$ Renal / bladder cancer: $n=5$ Colorectal cancer: $n=2$ Breast cancer: $n=2$ Lymphoma: $n=2$ Ductal adenocarcinoma of the pancreas: $n=2$ Esophagastric Junction Cancers (AEG): $n=2$ Cancer of unknown primary (CUP): $n=1$ Endometrial cancer: $n=1$	n.a	n.a
Lipid-rich vs. lipid-poor	n.a	Lipid-rich: $n=35$ (77.8%)	n.a
Mean lesion volume (mm <sup>3</sup> )	9757.53 (3493.1–11,510.3)	4626.2 (1140.4–6317.7)	0.001

BMI body mass index, CTDI computed tomography dose index, IQR interquartile range

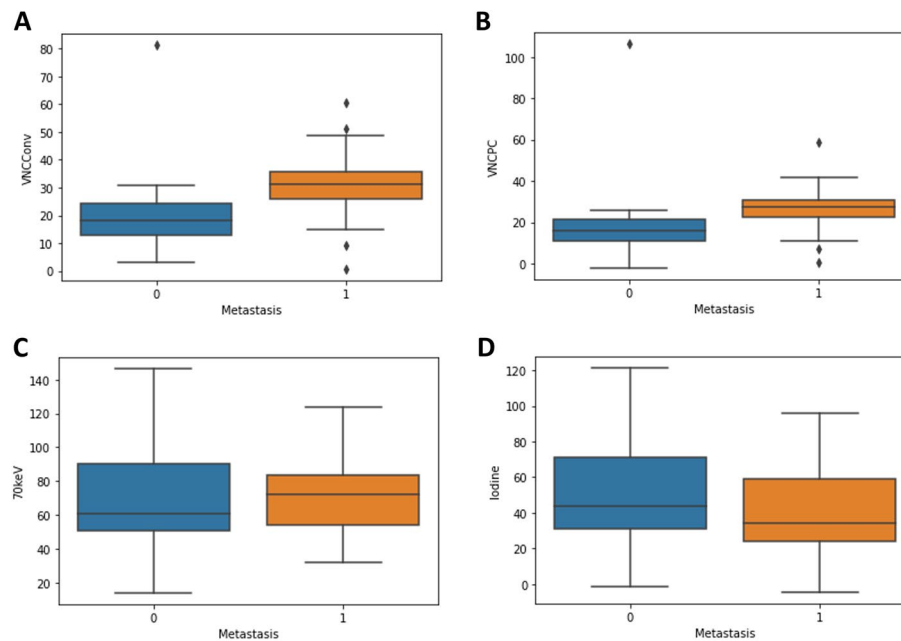


**Fig. 2** Boxplots for quantitative analyses of mean CT values **(A)**  $VNC_{Conv}$  ( $p = 0.007$ ), **(B)**  $VNC_{PC}$  ( $p = 0.007$ ), **(C)** 70 keV ( $p = 1.000$ ) and **(D)** iodine density maps ( $p = 0.726$ ) in adrenal lesions and differentiation between metastases and adenomas. 0 = no metastasis/adenoma; 1 = metastasis;  $VNC_{Conv}$  = conventional virtual non-contrast;  $VNC_{PC}$  = Virtual non-contrast pure calcium

**Table 2** Mean CT values at different reconstructions in metastasis and adenoma

	Metastasis	Adenoma	<i>p</i> value
40 keV	149.53 (106.61–218.87)	161.57 (120.27–245.01)	1.000
50 keV	110.42 (81.03–151.41)	111.60 (88.78–172.80)	1.000
60 keV	86.70 (67.02–109.59)	78.93 (65.59–121.20)	1.000
70 keV	72.09 (53.89–83.88)	60.78 (50.77–90.37)	1.000
80 keV	61.11 (46.43–69.44)	49.82 (41–69.98)	1.000
90 keV	54.06 (42.88–60.03)	42.88 (34.88–58.47)	0.296
Iodine maps	33.93 (23.93–58.80)	43.92 (30.74–71.31)	0.726
$VNC_{Conv}$	31.28 (26.00–35.89)	18.15 (12.92–24.26)	0.007
$VNC_{PC}$	27.22 (22.59–30.64)	16.00 (11.02–21.56)	0.007
TNC	19.12 (7.52–22.77)	4.28 (–3.24–7.11)	0.021

Data shown as median (interquartile range); *p* value shown after Bonferroni correction

$VNC$  virtual non-contrast,  $VNC_{Conv}$  conventional VNC algorithm,  $VNC_{PC}$  pure calcium VNC algorithm, TNC true non-contrast

showed an AUC of 0.762,  $VNC_{Conv}$  reconstructions showed an AUC of 0.857, and  $VNC_{PC}$  reconstructions an AUC of 0.931 in ROC analyses (Fig. 5). Table 4 gives an overview of different cutoff values for  $VNC_{Conv}$  and  $VNC_{PC}$  reconstructions and TNC and their sensitivity and specificity as well as accuracy and precision for discrimination between adenomas and metastases. Using for example 26 HU in the  $VNC_{Conv}$  reconstruction as a cutoff value, there is a sensitivity of 86.7% and a specificity of 75.6% for the correct diagnosis. For

TNC, an optimal cutoff value of 10.8 was observed in our cohort and showed best discrimination between benign and malignant adrenal lesions with a sensitivity of 71.4% and a specificity of 82.9%.

## Discussion

Although the mean differences to TNC are smaller on  $VNC_{PC}$  than on  $VNC_{Conv}$  series, there is still an overestimation of CT values in the assessment of adrenal lesions. Nevertheless, the use of VNC facilitates the discrimination of adenomas and metastases on contrast-enhanced scans, using a higher threshold for discrimination (e.g., 26 HU instead of the established 10 HU for TNC).

The diagnostic workup of incidental adrenal lesions on contrast-enhanced CT scans is a well-known challenge in radiology. In most cases, further imaging (e.g., adrenal CT or MRI) or follow-up is recommended. This leads to increased costs due to additional testing, which can also lead to increased radiation exposure and/or delayed diagnosis. In the era of DECT and PCD-CT, one might think that virtual non-contrast imaging could solve this problem. However, similar to previous studies on DECT, the first published experiences on PCD-CT also reported that VNC over- or underestimates CT values compared to TNC [1, 9, 20].

Therefore, VNC has not been recommended for routine clinical use because even a discreet discrepancy in CT values may have a significant impact on the diagnosis and further workup of adrenal lesions [4, 11]. Similar to previous studies, we also reported significant

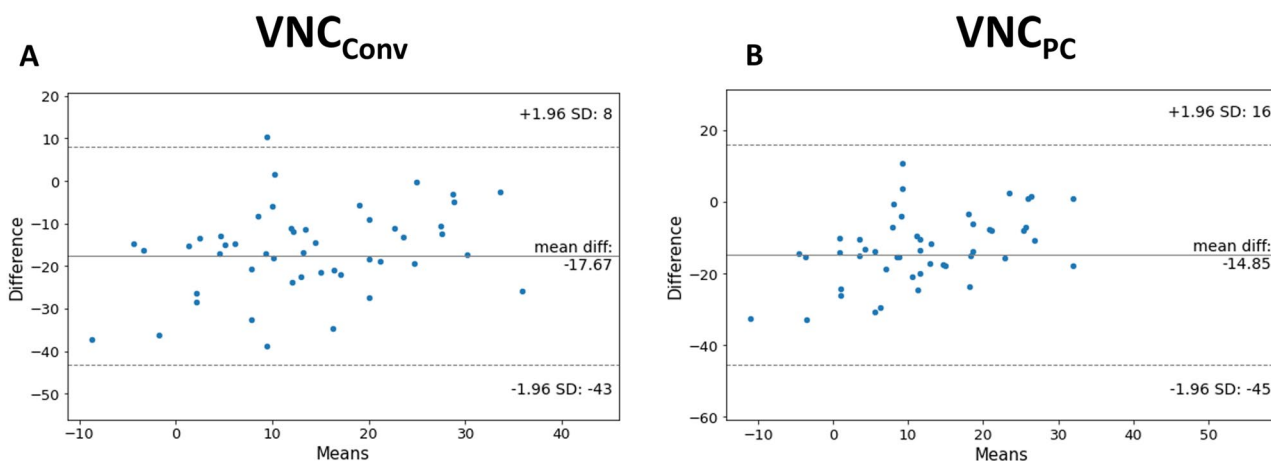


**Fig. 3** Bland Altman plots for difference between TNC and different VNC algorithms (**A** VNC<sub>Conv</sub> and **B** VNC<sub>PC</sub>) in the subgroup of patients with available TNC (*n* = 49). TNC = true non-contrast; VNC<sub>Conv</sub> = conventional virtual non-contrast; VNC<sub>PC</sub> = Virtual non-contrast pure calcium

**Table 3** Feature importance

	Mean importance	Median importance	Minimum importance	Maximum importance	Decision
40 keV	1.688556	1.688494	-0.57961552	4.320842	Rejected
50 keV	1.950700	1.926037	0.02061232	3.640417	Rejected
60 keV	2.358565	2.223441	-0.53112638	4.766701	Tentative
70 keV	1.911188	1.849627	-0.70735873	4.901965	Rejected
80 keV	3.405728	3.447088	0.90215446	6.125980	Confirmed
90 keV	5.585501	5.702772	1.76194257	8.457138	Confirmed
Iodine maps	3.491482	3.478601	0.70263658	5.992867	Confirmed
VNC <sub>Conv</sub>	19.038321	19.040796	16.09838496	22.228905	Confirmed
VNC <sub>PC</sub>	15.508909	15.486995	13.79535125	18.198172	Confirmed

VNC virtual non-contrast, VNC<sub>Conv</sub> conventional VNC algorithm, VNC<sub>PC</sub> pure calcium VNC algorithm

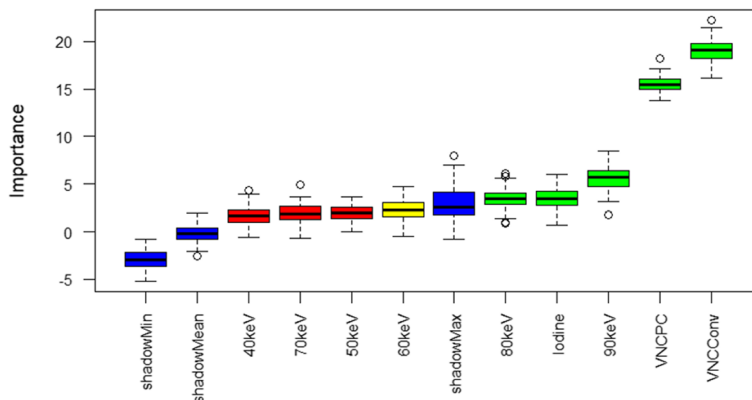


**Fig. 4** Feature importance in a Random Forest Model (Boruta)

overestimation of VNC<sub>Conv</sub> compared to TNC with a mean difference of about 17 HU.

In this study, we aimed also to assess the value of a new and promising VNC algorithm (VNC<sub>PC</sub>) in the diagnosis of adrenal lesions [13]. Whereas the discrepancy in CT

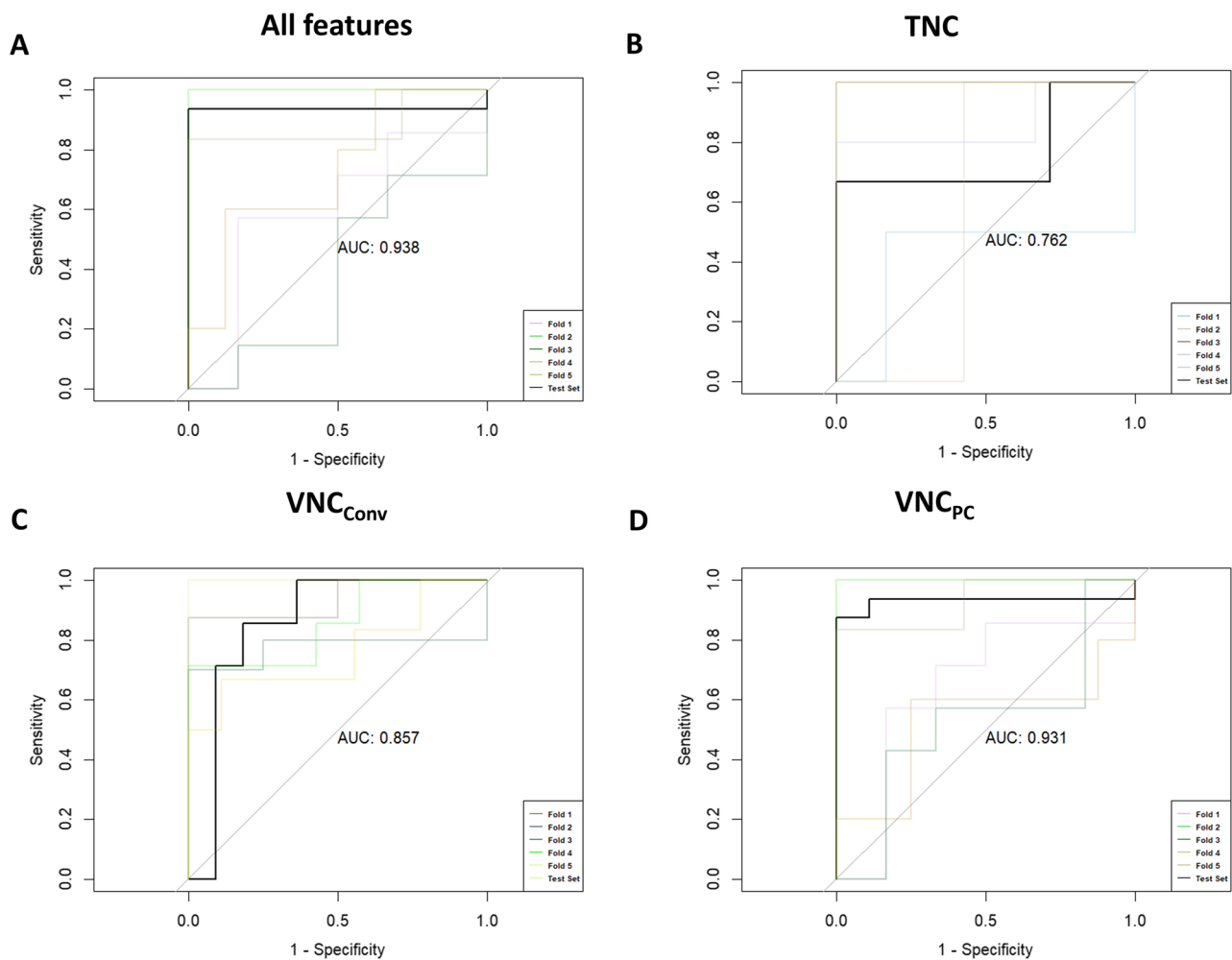


**Fig. 5** ROC analysis using metastasis as dependent variable and either **(A)** all features, **(B)** TNC, **(C)** VNC<sub>Conv</sub> or **(d)** VNC<sub>PC</sub> as independent variables. Data are shown for all five trained models (folds 1–5) and for the best model that was selected after validation and then applied to the test cohort (test set). AUC is shown for the model that was applied to the test cohort. TNC = true non-contrast; VNC<sub>Conv</sub> = conventional virtual non-contrast; VNC<sub>PC</sub> = Virtual non-contrast pure calcium

values compared to TNC is smaller using this new algorithm, there is still a mean difference of about 15 HU. A mean deviation of 15 HU might be too high in the assessment of adrenal adenomas and might entail incorrect diagnoses.

Therefore, it is necessary to address this problem in the near future and to improve algorithms of VNC. However, VNC reconstructions might still have value in clinical routine currently if a “new” (different) threshold for VNC reconstructions is agreed on. Logistic regression analyses in this work revealed higher optimal thresholds for VNC in the discrimination between adenomas and metastases. For example, using a threshold of 26 HU instead of the established 10 HU for TNC results in high sensitivity and specificity for differentiating between adenomas and metastases. In our study, specificity and

sensitivity were even higher using, e.g., 26 HU in VNC reconstructions compared to 10 HU in TNC. Our analyses reported different “optimal” cutoff values for VNC<sub>Conv</sub> and VNC<sub>PC</sub>, which are presented in Table 4. They differ regarding specificity and sensitivity. With lower HU values, sensitivity increases while specificity decreases and vice versa. In our opinion, 26 HU was the best “compromise” between specificity and sensitivity for VNC<sub>Conv</sub>. Therefore, we decided to choose this value. However, further studies with larger patient cohorts must confirm the results of this study and define the “final” optimal cutoff value. An integration of this threshold in clinical routine also requires further analyses; the findings of well-established 10 HU as the best threshold in TNC in our cohort support the validity of our examinations. Yet, one major challenge might be the standardization of the

**Table 4** Best cutoff values

Threshold	Specificity	Sensitivity	Accuracy	Precision
VNC <sub>PC</sub>				
21.8	80.0	77.8	78.9	79.6
22.5	82.2	75.6	78.9	80.9
22.9	84.4	73.3	78.9	82.5
23.4	86.7	71.1	78.9	84.2
24.4	91.1	66.7	78.9	88.2
VNC <sub>Conv</sub>				
25.2	82.2	80.0	81.1	81.8
25.8	84.4	77.8	81.1	83.3
26.0	86.7	75.6	81.1	85.0
27.3	88.9	73.3	81.1	86.8
28.5	93.3	68.9	81.1	91.2
29.4	95.6	66.7	81.1	93.8
TNC				
10.8	82.9	71.4	79.6	62.5

VNC virtual non-contrast, VNC<sub>PC</sub> pure calcium VNC algorithm, VNC<sub>Conv</sub> conventional VNC algorithm, TNC true non-contrast

results in VNC reconstructions. Due to rapid technical developments, different VNC algorithms exist. Therefore, standardization of VNC pipelines or alternatively a harmonization of data will be crucial aspects for upcoming studies with larger patient cohorts. Especially multicenter studies with consented protocols are necessary to confirm the results of this study and to redefine the threshold for the diagnosis of adrenal lesions in contrast-enhanced CT.

The present study also analyzed the value of different imaging features derived from spectral imaging (e.g., iodine maps, VMI) in discriminating between adrenal adenomas and metastases. A previous study on DECT showed promising results for the combination of iodine density and VNC [1]. Other studies have also highlighted the discriminative power of fat fraction and radiomics [7, 8].

To our knowledge, no previous studies have addressed the value of spectral imaging for the discrimination between adrenal adenomas and adrenal metastases. Our study shows that adrenal adenomas and metastases have significantly different imaging characteristics (e.g., adenomas have lower CT values in VNC<sub>Conv</sub> and VNC<sub>PC</sub> compared to metastases), which is similar to previously reported results on DECT [1].

Logistic regression analysis and random forest classifiers identified VNC (both VNC<sub>Conv</sub> and VNC<sub>PC</sub>) as the most important parameters in discriminating between adrenal adenomas and metastases.

In view of these results, it is very important to address the technical optimization of VNC algorithms to approximate CT values of TNC and/or the definition of a “new” (different) threshold for VNC. The possibility to safely replace TNC with VNC could save many CT or MRI scans in the workup of adrenal lesions, might accelerate the diagnosis, and potentially reduce psychological burden for the patients due to delayed clarification.

In contrast to the previous study on DECT [1] and also to the previous study on PCD-CT [11], we performed a complete 3D segmentation of the entire adrenal lesion and did not use only ROI-based measurements. We aimed to improve the diagnostic accuracy and avoid bias that may be introduced by ROI-based measurements. However, similar results with an over- and underestimation of CT values in VNC (compared to TNC) were also observed with this method. The spectral information used in this study is based on PCD-CT differentiating photon energy (above a certain level to eliminate electronic noise) in high and low, e.g., using one threshold to create two so-called bins. In the future, up to four bins (differentiation with three thresholds) will most likely be available according to the manufacturer. This could provide even more information, potentially leading to improved CT values in VNC reconstructions.

Body mass index (BMI) is known to affect image noise and image quality [21]. A previous study on PCD-CT showed that contrast-to-noise ratio (CNR) for detection of liver metastases did not differ in a wide range of BMI suggesting a preservation of CNR on a PCD-CT [22]. Similar results were also shown in a previous study analyzing the conspicuity of pancreatic ductal adenocarcinoma on a PCD-CT; this study also found no significant differences in CNR in portal venous phase for patients with higher and lower BMI [23]. The present study showed no significant differences in BMI between patients with adenomas and metastases; however, a tendency towards a lower BMI in the metastases cohort was observed. According to the results of the previous studies and the suggested CNR-preserving potential of PCD-CT in a wide range of BMI, we do not expect these findings to significantly influence the results of the present study (also due to the small patient cohort).

This study has limitations: first, this was a single-center study with inclusion of both—patients with known or suspected malignancies and multiphasic CT scans for assessment of adrenal lesions [24]. Second, TNC was only available for a subgroup of patients with a higher proportion of patients with adenomas which might introduce a bias. Third, the diagnosis of



adenomas or metastases was not confirmed histopathologically, but by either further imaging (e.g., adrenal CT, unenhanced CT, MRI) or follow-up.

## Conclusion

VNC reconstructions tend to overestimate CT values in comparison to TNC in the assessment of adrenal lesions. However, there is still a high diagnostic accuracy for both, the conventional and the new calcium-preserving VNC algorithm in the discrimination of adrenal lesions, especially when elevating the established threshold of 10 HU to about 26 HU. Therefore, a “new” threshold for VNC reconstructions may safely discriminate adrenal lesions and might save further workup of unclear cases. Further studies with larger patient cohorts and multi-center studies using standardized methodology and data harmonization are necessary to confirm the results of this study.

## Abbreviations

DECT	Dual-energy CT
keV	Kiloelectronvolt
PCD-CT	Photon-counting detector CT
TNC	True non-contrast
VMI	Virtual monoenergetic images
VNC <sub>Conv</sub>	Conventional virtual non-contrast
VNC <sub>PC</sub>	Virtual non-contrast pure calcium

## Funding

Open Access funding enabled and organized by Projekt DEAL. This work was partially supported by the University Augsburg. The open access publication of this article was supported by the DFG sponsored Open Access Fund of the University of Augsburg. The authors state that this work has not received any other (external) funding.

## Declarations

### Guarantor

The scientific guarantor of this publication is Josua Decker.

### Conflict of interest

The authors of this manuscript declare relationships with the following companies: Thomas Kröncke and Florian Schwarz are (unpaid) members of the “Photon Counting advisory board” of Siemens Healthineers.

The authors of this manuscript declare no other relationships with any companies, whose products or services may be related to the subject matter of the article.

### Statistics and biometry

Several authors have significant statistical expertise.

### Informed consent

Written informed consent was waived by the Institutional Review Board for retrospectively included patients.

### Ethical approval

Institutional Review Board approval was obtained by the Medical Research and Ethics Committee (MREC) of the Ludwig-Maximilians-University Munich (protocol number: 22–0456).

### Study subjects or cohorts overlap

The study subjects or cohorts have not been previously reported.

## Methodology

- retrospective
- diagnostic or prognostic study
- performed at one institution

## Author details

<sup>1</sup>Diagnostic and Interventional Radiology, University Hospital Augsburg, Faculty of Medicine, University of Augsburg, Stenglinstr. 2, 86156 Augsburg, Germany. <sup>2</sup>Diagnostic and Interventional Radiology, Donau-Isar-Klinikum, Perlaserger Str. 41, 94469 Deggendorf, Germany. <sup>3</sup>Institute of Digital Health, University Hospital Augsburg, Augsburg, Germany. <sup>4</sup>Computer-Aided Medical Procedures and Augmented Reality, School of Computation, Information and Technology, Technical University of Munich, Munich, Germany. <sup>5</sup>Centre for Advanced Analytics and Predictive Sciences (CAAPS), University of Augsburg, Universitätsstr. 2, 86159 Augsburg, Germany.

Received: 23 November 2023 Revised: 5 January 2024

Accepted: 7 February 2024 Published online: 14 March 2024

## References

1. Nagayama Y, Inoue T, Oda S et al (2020) Adrenal adenomas versus metastases: diagnostic performance of dual-energy spectral CT virtual noncontrast imaging and iodine maps. *Radiology* 296:324–332. <https://doi.org/10.1148/radiol.2020192227>
2. Pacak K, Eisenhofer G, Grossman A (2007) The incidentally discovered adrenal mass. *N Engl J Med* 356:2005. <https://doi.org/10.1056/NEJMc070612>
3. Bovio S, Cataldi A, Reimondo G et al (2006) Prevalence of adrenal incidentaloma in a contemporary computerized tomography series. *J Endocrinol Invest* 29:298–302. <https://doi.org/10.1007/BF03344099>
4. Mayo-Smith WW, Song JH, Boland GL et al (2017) Management of incidental adrenal masses: a white paper of the ACR Incidental Findings Committee. *J Am Coll Radiol* 14:1038–1044. <https://doi.org/10.1016/j.jacr.2017.05.001>
5. Sangwaiya MJ, Boland GWL, Cronin CG et al (2010) Incidental adrenal lesions: accuracy of characterization with contrast-enhanced washout multidetector CT–10-minute delayed imaging protocol revisited in a large patient cohort. *Radiology* 256:504–510. <https://doi.org/10.1148/radiol.10091386>
6. Caoili EM, Korobkin M, Francis IR et al (2002) Adrenal masses: characterization with combined unenhanced and delayed enhanced CT. *Radiology* 222:629–633. <https://doi.org/10.1148/radiol.2223010766>
7. Loonis A-ST, Yu H, Glazer DI et al (2023) Dual energy-derived metrics for differentiating adrenal adenomas from nonadenomas on single-phase contrast-enhanced CT. *AJR Am J Roentgenol* 220:693–704. <https://doi.org/10.2214/AJR.22.28323>
8. Winkelman MT, Gassenmaier S, Walter SS et al (2022) Differentiation of adrenal adenomas from adrenal metastases in single-phased staging dual-energy CT and radiomics. *Diagn Interv Radiol* 28:208–216. <https://doi.org/10.5152/dir.2022.21691>
9. Cao J, Lennartz S, Parakh A et al (2021) Dual-layer dual-energy CT for characterization of adrenal nodules: can virtual unenhanced images replace true unenhanced acquisitions? *Abdom Radiol (NY)* 46:4345–4352. <https://doi.org/10.1007/s00261-021-03062-3>
10. Flohr T, Petersilka M, Henning A et al (2020) Photon-counting CT review. *Phys Med* 79:126–136. <https://doi.org/10.1016/j.ejmp.2020.10.030>
11. Lennartz S, Schoenbeck D, Kröger JR et al (2023) Photon-counting CT material decomposition: initial experience in assessing adrenal adenoma. *Radiology* 306:202–204. <https://doi.org/10.1148/radiol.220919>
12. Risch F, Schwarz F, Braun F et al (2023) Assessment of epicardial adipose tissue on virtual non-contrast images derived from photon-counting detector coronary CTA datasets. *Eur Radiol* 33:2450–2460. <https://doi.org/10.1007/s00330-022-09257-6>
13. Decker JA, Bette S, Scheurig-Muenkler C et al (2022) Virtual non-contrast reconstructions of photon-counting detector CT angiography datasets as substitutes for true non-contrast acquisitions in patients after EVAR-performance of a novel calcium-preserving reconstruction algorithm.

- Diagnostics (Basel) 12(3):558. <https://doi.org/10.3390/diagnostics12030558>
14. Risch F, Bette S, Sinzinger A et al (2023) Multiphase photon counting detector CT data sets - which combination of contrast phase and virtual non-contrast algorithm is best suited to replace true non-contrast series in the assessment of active bleeding? *Eur J Radiol* 168:111125. <https://doi.org/10.1016/j.ejrad.2023.111125>
  15. Fedorov A, Beichel R, Kalpathy-Cramer J et al (2012) 3D Slicer as an image computing platform for the Quantitative Imaging Network. *Magn Reson Imaging* 30:1323–1341. <https://doi.org/10.1016/j.mri.2012.05.001>
  16. van Griethuysen JJM, Fedorov A, Parmar C et al (2017) Computational radiomics system to decode the radiographic phenotype. *Cancer Res* 77:e104–e107. <https://doi.org/10.1158/0008-5472.CAN-17-0339>
  17. R Core Team (2014) R Development Core Team. R: a language and environment for statistical computing. R Foundation for Statistical Computing. Vienna, Austria
  18. RStudio Team (2020) RStudio: integrated development environment for R. RStudio. PBC; Boston, MA, USA
  19. Ayx I, Tharmaseelan H, Hertel A et al (2022) Myocardial radiomics texture features associated with increased coronary calcium score—first results of a photon-counting CT. *Diagnostics (Basel)* 12(7):1663 <https://doi.org/10.3390/diagnostics12071663>
  20. Shern Liang E, Wastney T, Dobeli K, Hacking C (2022) Virtual non-contrast detector-based spectral CT predictably overestimates tissue density for the characterisation of adrenal lesions compared to true non-contrast CT. *Abdom Radiol (NY)* 47:2462–2467. <https://doi.org/10.1007/s00261-022-03528-y>
  21. Qurashi AA, Rainford LA, Alshamrani KM, Foley SJ (2019) The impact of obesity on abdominal CT radiation dose and image quality. *Radiat Prot Dosimetry* 185:17–26. <https://doi.org/10.1093/rpd/ncy212>
  22. Bette S, Decker JA, Braun FM et al (2022) Optimal conspicuity of liver metastases in virtual monochromatic imaging reconstructions on a novel photon-counting detector CT—effect of keV settings and BMI. *Diagnostics (Basel)* 12(5):1231. <https://doi.org/10.3390/diagnostics12051231>
  23. Decker JA, Becker J, Härting M et al (2023) Optimal conspicuity of pancreatic ductal adenocarcinoma in virtual monochromatic imaging reconstructions on a photon-counting detector CT: comparison to conventional MDCT. *Abdom Radiol (NY)*. <https://doi.org/10.1007/s00261-023-04042-5>
  24. Nagayama Y, Hirai T (2023) Diagnostic performance of contrast-enhanced dual-energy CT metrics for differentiating adrenal adenomas from nonadenomas can be affected by inclusion criteria. *AJR Am J Roentgenol* 221(2):285. <https://doi.org/10.2214/AJR.23.29073>

### Publisher's note

Springer Nature remains neutral with regard to jurisdictional claims in published maps and institutional affiliations.